Hydration Characteristics and Evolution Strength Rules During the Early Curing Stage of Backfill Slurry at High Temperatures

Yuye Tan[1,2,*], Yuchao Deng[1,2], Davide Elmo[3], Fenghao Zhu[1,2], Jiazhao Chen[1,2], and Weidong Song[1,2]

[1]State Key Laboratory of High-Efficient Mining and Safety of Metal Mines of Ministry of Education, University of Science and Technology Beijing, Beijing, 100083, China; tanyuye@ustb.edu.cn (Y.T.); M202320066@xs.ustb.edu.cn (Y.D.); 13476693596@163.com (F.Z.); cjzgzyx2021@163.com (J.C.); songwd@ustb.edu.cn (W.S.)

[2]School of Civil and Resource Engineering, University of Science and Technology Beijing, Beijing 100083, China

[3]NBK Institute of Mining Engineering, University of British Columbia, Vancouver, BC V6T 1Z4, Canada; delmo@mining.ubc.ca(D.E.)

*Correspondence: tanyuye@ustb.edu.cn (Y.T.)

Abstract

With the gradual depletion of surface and shallow mineral resources, deep mining has become the trend of future mining development. In the process of deep mining, the temperature will increase with the increase of mining depth, and will have a significant impact on the hydration reaction rate and products of the backfill; this changes the physical and mechanical properties of the backfill and affects backfill stability in the underground stope. In this study, the unclassified tailings of a gold mine and ordinary Portland cement were used as filling materials. By means of nuclear magnetic resonance (NMR) analysis, scanning electron microscope (SEM) observation, and a uniaxial compression experiment and theoretical analysis, the characteristics in the early curing stage of the unclassified tailings backfill slurry under high temperature conditions and the evolution strength rules of the backfill were explored. The results show that an increase of temperature leads to decrease of porosity in backfill slurry, decrease of free water content, and an increase of adsorbed water and pore water content. Increasing the curing temperature can increase the degree of hydration reaction such that the hydration products of the backfill form a denser structure; this eventually leads to the increase of the strength of the backfill. These research results have important theoretical significance for the strength design of backfill in deep mining.

Key words: porosity, moisture content, hydration products, backfill strength

Introduction

Shallow mineral resources are gradually depleting, and deep mining has become the current development trend (Li et al.,2017; Cai et al., 2019; Cheng et al., 2021). In the process of underground metal mining, as depth increases, a series of challenges such as high ground pressure (Gao et al., 2015), high temperature (Wu et al., 2021), and poor stability of ore and rock (Liu et al., 2021) are faced. Cemented paste backfill mining, characterized by its efficiency and safety, has been widely applied in the deep metal mining process (Naguleswaran et al., 2015; Cao et al., 2019). In underground environments, temperature and humidity differences strongly affect the rate of free water conversion and ion diffusion within the backfill, ultimately causing variations in backfill strength (Chen et al., 2020).

Currently, research on the influence of temperature on the physical and mechanical properties of backfill materials is primarily conducted through indoor experiments (Liu et al., 2020; Cao et al., 2023), theoretical analyses (Cai and Wu, 2015), and numerical simulations (Bai et al., 2020). Some scholars have investigated the effects of factors such as cement-to-tailing ratio, curing temperature, and curing age on the physical properties (eg, slump, thermal expansion coefficient) and mechanical properties (eg, compressive strength, stress-strain curve, elastic modulus) of backfill materials through indoor experiments. They have established regression equations between various factors and the strength of backfill materials through multiple regression analyses, or utilized response surface methodology to calculate the response surface regression model of the influence of curing temperature and cement-to-tailing ratio on the strength of backfill materials theoretically (Ma et al., 2013; Bian et al., 2015; Han, 2015; Xiong, 2015). It was found that within a certain temperature range, the mechanical properties of backfill materials increase with increasing temperature (Han et al., 2015; Hao et al., 2020; Wang and Zhou, 2022), but higher curing temperatures may decrease the later strength of backfill materials (Fang and Fall, 2018). However, some studies have also found that compared to standard curing, low-temperature curing results in higher early strength of backfill materials (Hou et al., 2020; Pan et al., 2022). Some researchers have conducted experiments from a microscopic perspective to explore the influence of temperature on the macroscopic mechanical properties of backfill materials and explain the reasons for changes in backfill strength (Jiang, 2020).

Key techniques for studying the microstructure of backfill include SEM experiments to observe hydration products (Tan et al., 2020; Wang et al., 2020), as well as NMR experiments or mercury intrusion porosimetry to measure the porosity of the backfill (Jiang et al., 2022). NMR experiments can reveal the distribution of all pores but cannot provide information about pore morphology and specific surface area, two structural details of pores. On the other hand, mercury intrusion porosimetry reflects only a portion of the pore distribution and may also lead to damage to the pore structure of backfill due to elastic compression effects. The differences between these methods highlight the degree of pore connectivity (Kong and Zhang, 2013). Scholars integrated computed tomography scanning data and Avizo three-dimensional reconstruction software to reproduce the spatial distribution patterns of cracks and pores in backfill specimens after failure (Long et al., 2021). Under different curing conditions, the hydration products of the backfill mainly include ettringite (AFt) and calcium silicate hydrate (C-S-H) gel, and there are differences in the pore size distribution and compactness of their microstructures; for fiber-reinforced tailings paste backfill, higher curing temperatures lead to a reduction in the porosity of the backfill, thereby increasing the strength of the samples (Li et al. 2019).

A series of research achievements have been obtained regarding the relationship between the hydration process of backfill material and its strength. However, the factors involved in the hydration reaction are numerous, including hydration heat, moisture content and distribution, porosity, etc. This study investigates the variations in hydration process parameters of backfill material under different curing temperatures and correlates them with the macroscopic mechanical properties of the backfill. This holds significant importance for deep well backfill mining. A thorough understanding of how these parameter

variations affect the strength of the backfill material contributes to optimizing the design of backfill parameters, enhancing the overall performance and stability of the backfill.

Experimental material and Scheme

Experimental materials

The present experiment utilized unclassified tailings from a specific gold mine, PO42.5 ordinary Portland cement, and tap water as experimental materials. LS-POP(9) laser particle size analyzer and anhydrous ethanol were employed for particle size analysis of both the unclassified tailings and the cement to prevent the cement from dissolving. Particle size analyses were conducted on both the tailings and the cement, with the particle size distribution depicted in Figure 1. The average particle size of the tailings was determined to be 35.58 μm, while that of the cement was 24.53 μm.

Chemical compositions of the experimental materials are illustrated in Figure 2, and the X-ray diffraction (XRD) patterns in Figure 3. Based on Figures 2 and 3, the primary chemical constituents of the tailings are SiO_2 and Al_2O_3, whereas the cement is predominantly composed of CaO and SiO_2. The mineral composition of the tailings is relatively straightforward, encompassing substances such as quartz, feldspar, and zeolite. In contrast, the cement consists mainly of silicate minerals, including tricalcium silicate (C_3S), dicalcium silicate (C_2S), and tricalcium aluminate (C_3A). Throughout the hydration process, the gradual formation of C-S-H gel occurs, imparting strength and stability to the filling material. This experiment provides a comprehensive exploration of the physical, chemical, and mineralogical characteristics of the selected materials.

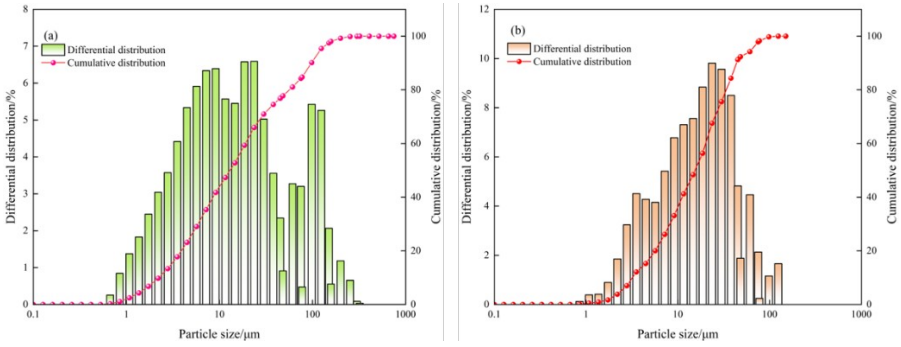

Figure 1. Particle size analysis of a) tailings, and b) cement.

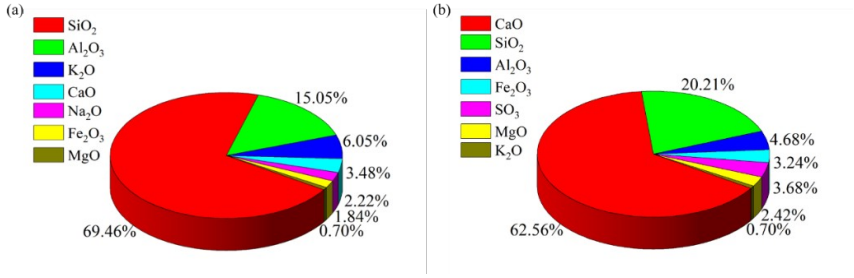

Figure 2. Chemical composition analysis of tailings (a) and cement (b).

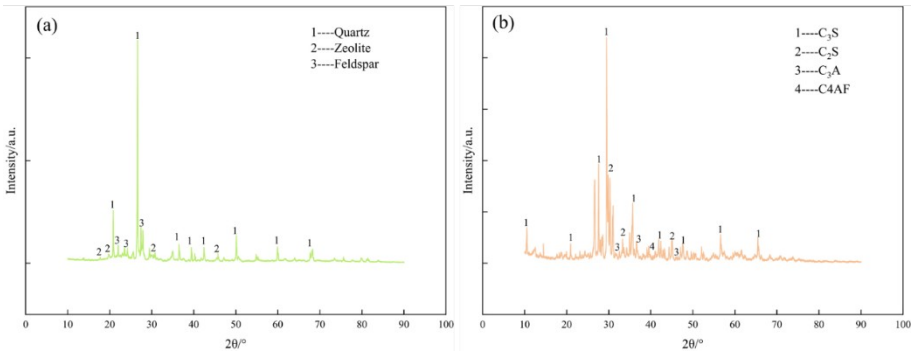

Figure 3. XRD spectra of a) tailings, and b) cement.

Experimental scheme

In accordance with a cement-to-tailings mass ratio of 1:6, appropriate amounts of ordinary Portland cement and unclassified tailings were accurately weighed. Subsequently, a suitable quantity of tap water was introduced for thorough mixing, resulting in the formation of a backfill slurry with a mass concentration of 65%. This slurry was then subjected to curing within a cement rapid curing chamber, with temperatures of 20, 30, 45, 65, and 75°C selected as curing temperatures. Temperature differentials were meticulously controlled within a range of ±2°C. The standard curing temperature for the filling material was maintained at around 20°C; therefore, temperatures of 30°C and above were considered elevated temperatures in the context of this study.

NMR analysis experiment

This experiment employed the Suzhou Niumai MesoMR23-060H-I NMR analysis system for testing, NMR technology can non-destructively measure the pore structure of saturated samples such as backfill slurry. To minimize experimental errors, three samples were prepared for each curing temperature, resulting in a total of 15 samples. The prepared backfill slurry was placed into 20 mL covered cylindrical glass bottles. To investigate the early hydration characteristics of the backfill slurry, a curing age of three days was selected. Due to large changes in porosity and moisture content shortly after the preparation of the backfill slurry, frequent testing of the samples was necessary in the initial stages. Therefore, within the cement rapid curing chamber, the backfill slurry underwent curing for 0, 1, 2, 4, 10, 24, 48, and 72 hrs. After completion of the curing process, the samples were retrieved and subjected to NMR testing.

Hydration product observation experiment

The experiments were conducted using the Carl Zeiss tungsten filament SEM to observe the microscopic morphology of the backfill at different curing temperatures (20, 30, 45, 65, and 75°C) and various curing ages (3, 7, and 14 days). The backfill sample was cut along the section to make its size about 5 × 10 × 10 mm. The sample was packaged with conductive copper foil and a relatively flat section was selected for observation. In order to meet the requirements of the experimental test, reduce the influence of negative charge on the imaging effect, and improve conductivity, the sample was dried and carbon sprayed before the experiment.

UCS test experiment

The UCS of backfill specimens was tested using a uniaxial compression testing machine. The backfill specimens were cured for a specific duration at all previously specified temperatures. Three tests were conducted for each curing condition, with a loading speed set at 0.5 mm/min. The experimental equipment and procedure are illustrated in Figure 4.

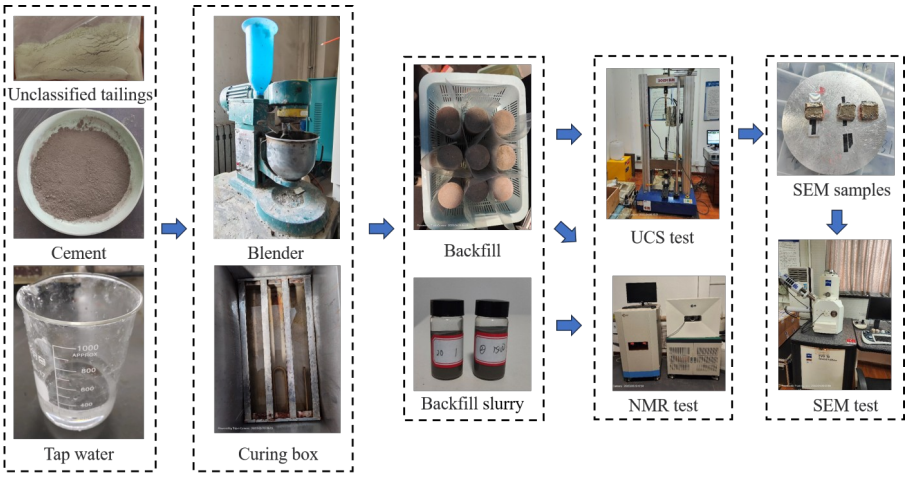

Figure 4. Experimental equipment and process.

Experimental Results and Analysis

Hydration characteristics during the early curing stage of the unclassified tailings backfill slurry at high temperatures

Evolution of pore structure in backfill slurry during the early curing stage of hydration

Figure 5 illustrates the pore size distribution of the backfill slurry after 4, 24, 48, and 72 hrs of hydration at different curing temperatures. The pore size distribution of the backfill slurry can be categorized into three peaks, referred to as Peaks I, II, and III. The proportional areas of these peaks represent the content of pores at corresponding size ranges.

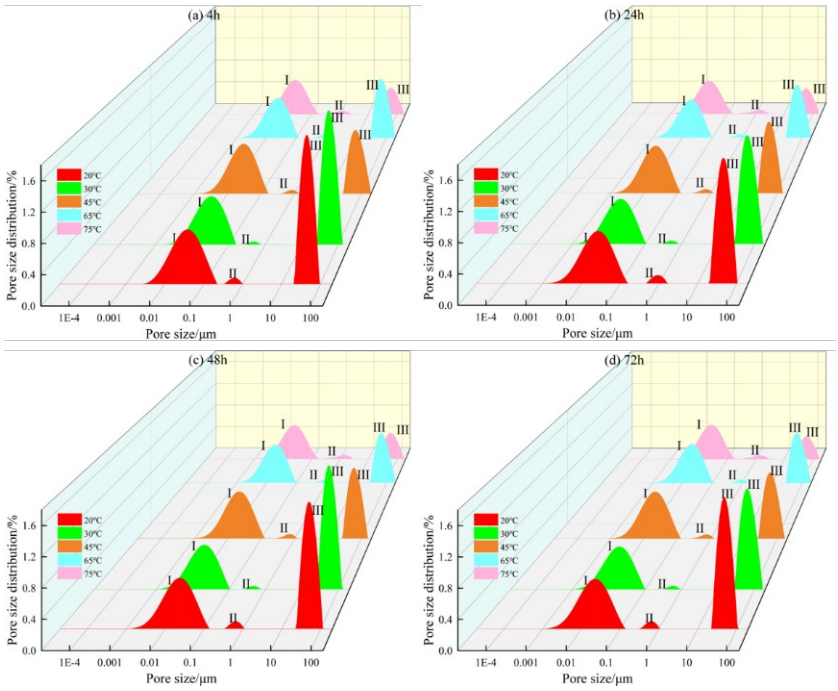

Figure 5. Pore size distribution of backfill slurry at a) 4 hrs, b) 24 hrs, c) 48 hrs, and d) 72 hrs.

With the increase in curing temperature the area of Peak I remains relatively unchanged, while the area of Peak III shows a gradual decrease (Figure 5). This indicates that with the rise in curing temperature, the content of small pores in the backfill slurry remains essentially constant, while the content of larger pores decreases. In other words, the porosity of the backfill decreases as the curing temperature rises. The observed phenomenon is likely attributed to the elevated curing temperature promoting moisture evaporation and release, thereby accelerating the hydration process. The release of moisture leads to the formation of pores and changes in pore size.

The results of porosity measurements on the backfill slurry obtained from NMR experiments are depicted in Figure 6. It is observed from the figure that, with increasing time, the porosity of the backfill slurry generally exhibits a decreasing trend. Moreover, under the same curing time, higher curing temperatures correspond to smaller porosities in the backfill slurry. This suggests that higher curing temperatures facilitate the promotion of hydration reactions in the backfill slurry, accelerating the formation of cementitious materials. This results in a denser pore structure within the backfill slurry, leading to a reduction in porosity.

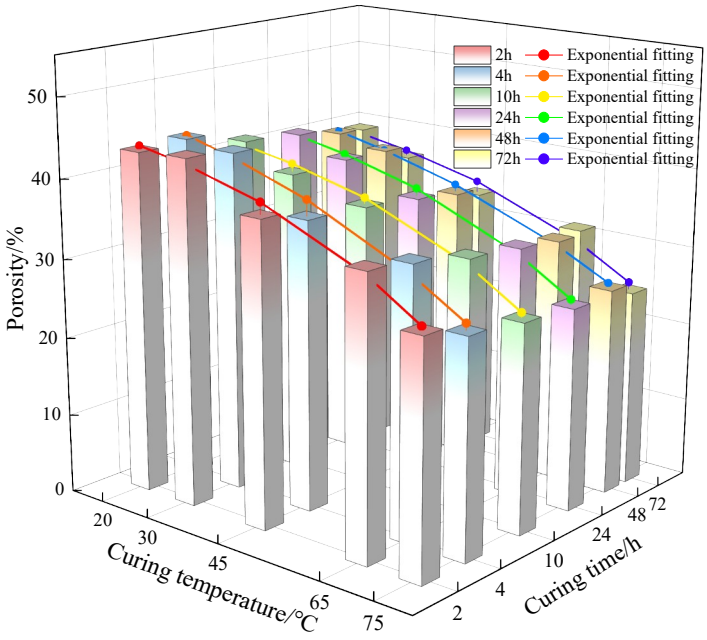

Figure 6. Curing time-curing temperature-backfill slurry porosity relationship.

At specific curing times, the relationship between the porosity of the backfill slurry and the curing temperature was investigated. The experimental results were fitted using relevant software. Fitting the experimental results reveals an exponential relationship between the porosity of the backfill slurry and temperature Table 1). The R^2 values indicate the reliability of the fitting results. Hence, it can be observed that results possess a certain level of persuasiveness.

Table 1. Fitting relationship between backfill slurry porosity and curing temperature.

Curing time/h	Fitting curve (POR/%, T/℃)	R^2
2	$POR = -2.316e^{\frac{T}{35.565}} + 47.362$	0.928
4	$POR = -5.348e^{\frac{T}{50.889}} + 51.569$	0.897
10	$POR = -1.855e^{\frac{T}{33.973}} + 43.900$	0.934
24	$POR = -2.519e^{\frac{T}{37.921}} + 44.543$	0.957
48	$POR = -4.811e^{\frac{T}{52.548}} + 46.717$	0.970
72	$POR = -2.241e^{\frac{T}{37.337}} + 42.444$	0.885

Temporal evolution of moisture content during the early hydration process of backfill slurry

Figure 7 displays the transverse relaxation time (T2) distribution of the backfill slurry at 20 and 65°C. The backfill slurry, characterized as a suspension containing solid particles, encompasses various forms of

water, including free water, adsorbed water, pore water, and chemically bound water. Due to the extremely short T2 of chemically bound water, NMR technology is generally considered incapable of directly detecting signals from chemically bound water. Shorter T2 periods are indicative of lower fluidity; thus, Peaks I, II, and III correspond to NMR signals of adsorbed water, pore water, and free water, respectively (Fu et al., 2023).

In comparison, at a curing temperature of 20°C, with the increase in curing time, the area of Peak I initially decreases before slowly changing, the area of Peak II remains relatively constant, and the area of Peak III increases. However, at a curing temperature of 65°C the areas of Peaks I and II remain essentially unchanged, while the area of Peak III decreases. This indicates that high-temperature curing alters the hydration process of the backfill, affecting the moisture variation and leading to a reduction in free water content.

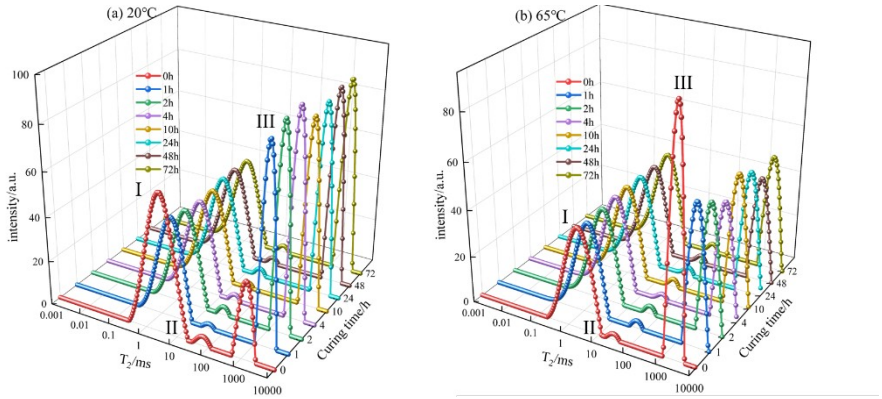

Figure 7. Inversion curves of T2 spectra for backfill slurry at a) 20℃, and b) 65℃.

Figure 8 depicts the variation curves of T2 peak areas in the backfill slurry at different curing temperatures. The T2 peak area is proportional to the various moisture contents in the backfill slurry (Song et al., 2022). Figures a, b, c, and d illustrate the changes in total moisture content, adsorbed water content, pore water content, and free water content, respectively. Analyzing Figure 8 reveals that high-temperature curing enhances the degree of hydration, leading to a reduction in the total moisture content of the backfill slurry. Furthermore, as the temperature increases, the extent of reduction in total moisture content initially increases, then decreases, followed by another increase. The temperature of 45°C serves as a turning point, where large changes occur in the adsorbed water content while other moisture content variations remain comparatively small. After curing the backfill slurry for 72 hrs, with the increase in curing temperature the pore water content of the backfill slurry increases. The adsorbed water content shows a slight upward trend, while the free water content decreases greatly, resulting in an overall reduction in total moisture content.

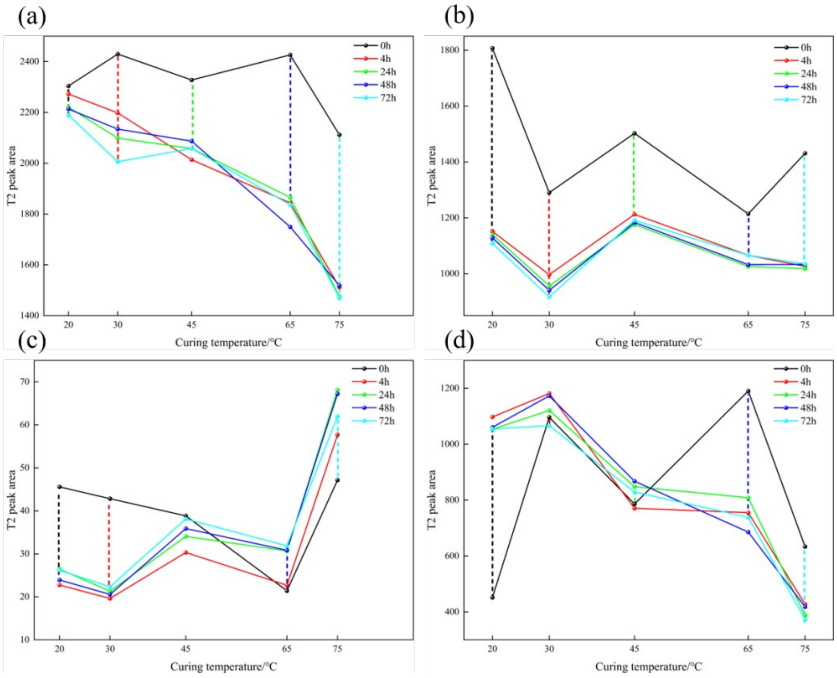

Figure 8. Curves depicting the variation in T2 peak area of the backfill slurry for a) total peak, b) Peak I, c) Peak II, and d) Peak III.

Hydration products and microstructure characteristics during the early curing stage of backfill

Figures 9 and 10 depict the microstructure of the backfill under room temperature and elevated temperature curing, respectively. The hydration products in the backfill primarily include C-S-H gel and AFt (Deng et al., 2023). In Figure 9(a), under room temperature curing for 3 days, small needle-like ettringite crystals appear on the surface of the backfill. These crystals exhibit a dispersed morphology, with relatively small but distinct sizes, and some pores are observable. The formation of layered gel is not yet pronounced. As shown in Figure 9(b), after 14 days of curing the needle-like ettringite crystals on the surface of the backfill further increase in both quantity and size. These crystals present a more distinct morphology, aggregating within the pores of the backfill. Additionally, small layered structures can be observed covering the pore walls of the backfill.

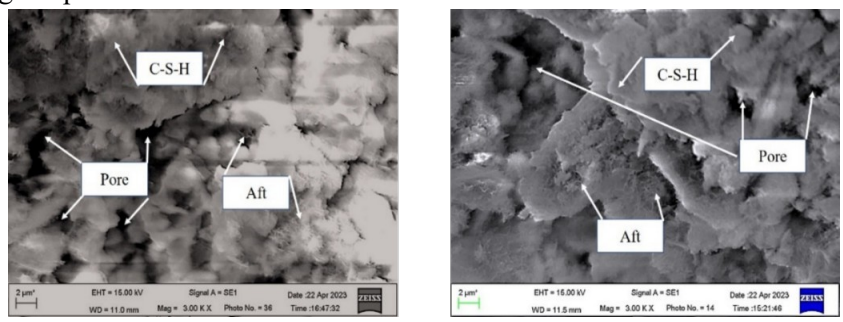

(a) 3d (b) 14d

Figure 9. Microstructure characteristics of the backfill at a curing temperature of 20 ℃.

Under high-temperature curing, the specimens with a 3 day curing age are primarily composed of C-S-H gel, exhibiting a well-developed gel structure (Figure 10). However, the needle-like ettringite crystals are not as prominent, which may be related to the observed locations. Figure 10(b) illustrates the microstructure of the backfill after 14 days of curing under elevated temperature conditions. The needle-like ettringite crystals on the surface of the backfill continue to grow and aggregate but are enveloped by the gel. Simultaneously, the layered C-S-H gel further develops, forming a relatively dense overall structure, indicating an enhanced degree of hydration.

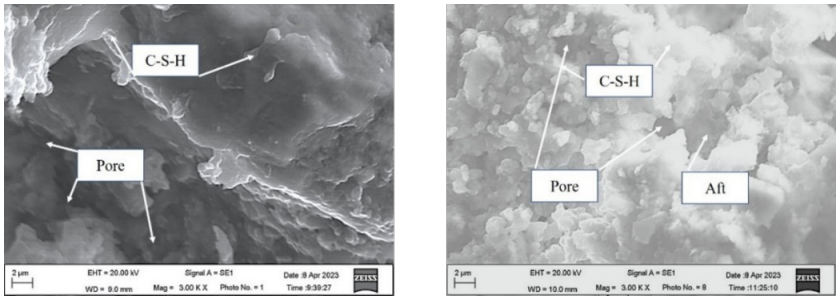

(a) 3d (b) 14d

Figure 10. Microstructure characteristics of the backfill at a curing temperature of 75 ℃ after a) 3 days and b) 14 days.

Under different curing durations at two distinct curing temperatures, the quantity and size of needle-like ettringite crystals on the surface of the backfill increase, and the degree of formation of layered C-S-H gel gradually intensifies. Particularly, under elevated-temperature curing conditions (eg, 75°C), the formation of layered C-S-H gel becomes more prominent. These observations indicate the strong influence of temperature on formation and growth of hydration products in the backfill. At higher temperatures, the hydration reaction proceeds more rapidly, favoring the formation and aggregation of C-S-H gel, resulting in a denser layer of C-S-H gel on the surface and pore walls of the backfill.

Mechanical properties of unclassified tailings cemented backfill at high temperatures

Strength evolution of unclassified tailings cemented backfill at high temperatures

Figure 11 illustrates the trend of uniaxial compressive strength of backfill specimens with varying curing temperatures. Under the same curing period, the uniaxial compressive strength of the backfill generally exhibits an increasing trend with rising curing temperatures. Taking curing temperatures of 20 and 75°C as examples, at a curing period of 3 days, the uniaxial compressive strength increased by 0.70 MPa. Meanwhile, at a curing period of 14 days, it increased by 1.68 MPa. This indicates that the curing temperature contributes to enhancing the early strength of the backfill. As established in previous studies, higher curing temperatures can accelerate the migration and transport of water, consequently expediting the progress of hydration reactions. This, in turn, promotes the quicker formation and development of cementitious materials, resulting in a denser and more ordered crystalline structure, thereby enhancing the early strength of the backfill.

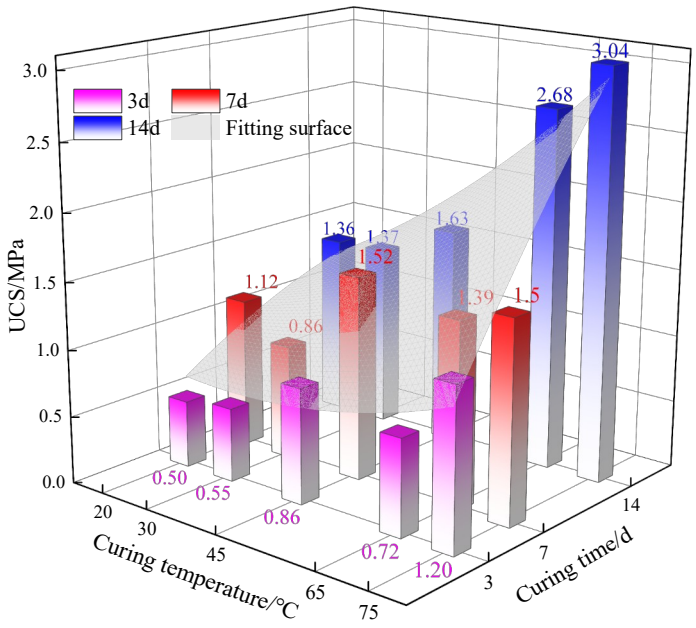

Figure 11. Curing time-curing temperature-backfill UCS relationship.

To investigate the relationship between the UCS of the backfill and curing temperature as well as curing time, the experimental results were subjected to nonlinear surface fitting using relevant software, the following relationship was obtained:

$$UCS = 0.68743 - 0.02092 \times T + 0.04479 \times t + 0.00018 \times T^2 - 0.00205 \times t^2 + 0.00221 \times T \times t \quad \text{Equation 1}$$

In Equation 1, UCS represents the uniaxial compressive strength of the backfill in MPa, T represents the curing temperature in ℃, t represents the curing time in days, and the fitting coefficient R^2 is 0.89. It can be considered that the relationship between the UCS of the backfill and the curing temperature, as well as the curing time, conforms to the aforementioned functional form.

Stress–strain curve characteristics of the backfill at high temperature

Figure 12 presents the stress-strain curves of the backfill under uniaxial loading conditions at temperatures of 20 and 75°C. The stress of the backfill increases with the growth of strain, but after reaching peak stress, it decreases with further strain. The uniaxial compressive failure process of the backfill can be divided into four stages:

1. Pore fissure compaction stage
2. Growth stage
3. Peak stage
4. Decay stage

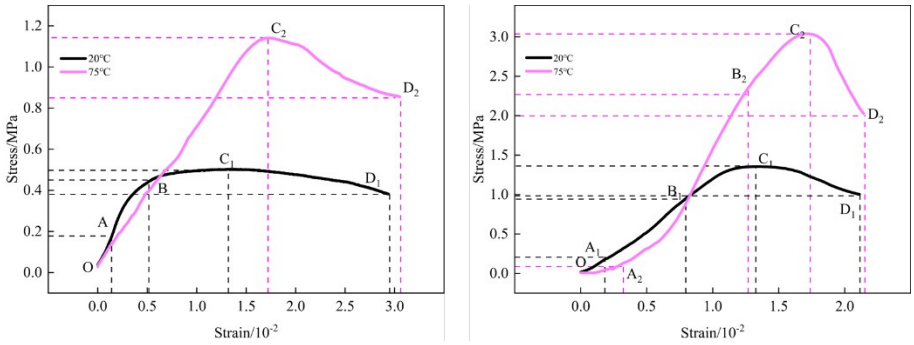

(a) 3d (b) 14d

Figure 12. Stress-strain curve of the backfill at curing temperatures of 20 and 75 ℃.

The pore fissure compaction stage (OA) is the initial phase following the application of load to the backfill. During this stage, the backfill begins to bear external loads, and strain increases with the rising stress. Tiny pores in the backfill commence densifying and deforming. In the growth stage (AB), the stress-strain curve exhibits an ascending trend. The backfill continues to withstand external loads, and stress increases with strain. Microcracks appear, resulting in increased inter-particle contact forces during this stage. The peak stage (BC) marks the highest point on the stress-strain curve. The backfill stress reaches its maximum value, and microcracks continuously aggregate, forming macroscopic fissures until complete failure. During the decay stage (CD), the stress-strain curve begins to decline. Macroscopic fissures rapidly develop, intertwining and forming a macroscopic fracture surface. However, the backfill still maintains a certain bearing capacity, and the stress value does not drop to zero.

In Figure 12, it can be observed that regardless of a curing duration of 3 or 14 days, the slopes of the peak stage (BC) and decay stage (CD) curves are higher under high-temperature curing compared to those under normal-temperature curing. This phenomenon arises because the curing temperature can influence the mechanical properties of the backfill, including strength, stiffness, and deformation characteristics, resulting in a variation in the elastic modulus of the backfill. Furthermore, different curing temperatures may induce variations in the internal structure and crystal arrangement of the backfill, ultimately impacting the shape of the stress-strain curve. These disparities indicate that the uniaxial compressive failure of the backfill under different curing temperatures may not involve the same type of damage process.

Damage characteristics of the backfill at high temperature

The failure characteristics of the backfill after uniaxial compression are illustrated in Figure 13. The primary failure mode of the backfill under uniaxial compression is characterized by conjugate shear failure, with a minor occurrence of tensile failure. Figures 13 a, b, c, and d depict shear failures. Under axial stress, the shear stress on the failure surface exceeds the maximum shear stress it can withstand, resulting in shear failure along the failure surface. Figure 13e represents tensile failure. Under axial stress, the backfill experiences tensile stress laterally, leading to failure and the development of longitudinal

macro-cracks. It is evident that elevating the curing temperature transitions the failure mode of the cemented backfill from shear failure to tensile failure. This transition may be attributed to the fact that under high-temperature curing, the hydration products of the backfill have formed a more stable structure, making it more prone to stress concentration phenomena.

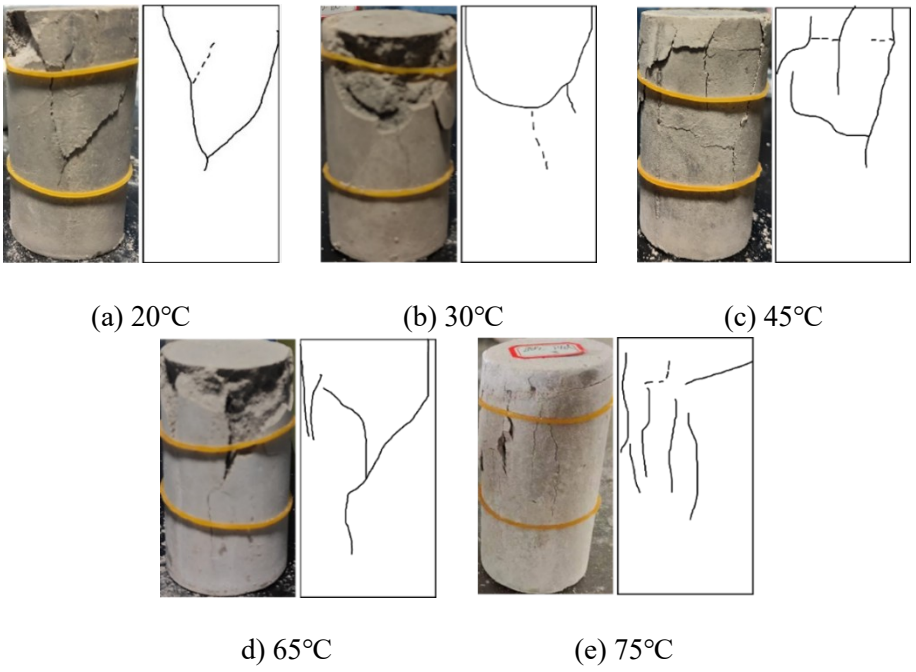

Figure 13. Deformation and failure characteristics of the backfill after 14 days of curing.

Conclusions

This research investigates the hydration characteristics and evolution strength rules during the early curing stage of backfill slurry at high temperatures, using the unclassified tailings from a gold mine and ordinary Portland cement as filling materials. Through theoretical analysis based on indoor experiments, the main research conclusions are as follows:

1. The physicochemical characteristics test results of the filling materials indicate that weighted average particle size of the unclassified tailings is 35.58 μm, with quartz being the predominant mineral along with major oxides including silicon dioxide and aluminum oxide. The weighted average particle size of the ordinary Portland cement is 24.53 μm and primarily composed of silicate minerals. Both the unclassified tailings and ordinary Portland cement are suitable as underground filling materials.
2. With the increase in curing temperature, the porosity of the backfill slurry generally shows a decreasing trend. Total moisture content decreases, pore water content slightly increases, adsorbed water content slightly rises, and free water content dramatically decreases. High-temperature curing alters the hydration process of the backfill slurry, accelerating the early hydration reaction of the backfill slurry.

3. The hydration products formed by the reaction between unclassified tailings and cement are mainly composed of C-S-H gel, ettringite, and other substances. SEM scans indicate that high-temperature curing results in more well-defined crystal morphologies of hydration products within the backfill, with a denser pore structure and smaller pore sizes.
4. High-temperature curing enhances the early strength of the backfill. When subjected to axial loading, the backfill undergoes stages of pore fissure compaction, growth, peak, and decay. Elevated curing temperatures alter the deformation characteristics of the backfill. An increase in curing temperature transitions the uniaxial failure mode of the backfill from shear failure to tensile failure.

Acknowledgements

This work was funded by the National Natural Science Foundation of China [52274110], the Growth Program for Young Teachers at Beijing University of Science and Technology (QNXM20220004), the National Natural Science Foundation of China [52004019], and the China Scholarship Cuncil fund (202206465005).

References

Li X.B., Wang S.F., Zhou J., et al. (2017) Review and practice of deep mining for solid mineral resources. The Chinese Journal of Nonferrous Metals, Vol. 27, pp. 1236-1262. https://doi.org/10.19476/j.ysxb.1004.0609.2017.06.021

Cai M.F., Ren F.H., Xue D.L. (2019) Current status and development strategy of metal mines. Chinese Journal of Engineering, Vol. 41, pp. 417-426. https://doi.org/10.13374/j.issn2095-9389.2019.04.001

Cheng, J.Z., Huang L.Q., Zhou J., et al. (2021) Practice and thought on sustainable development of nonferrous metal mining. The Chinese Journal of Nonferrous Metals, Vol. 31, pp. 3436-3449. https://doi.org/10.11817/j.ysxb.1004.0609.2021-42049

Gao F., Ju Y., Xie H.P. (2015) Research and Development of Rock mechanics in Deep ground engineering. Chinese Journal of Rock Mechanics and Engineering, Vol. 34, pp. 2161-2178. https://doi.org/10.13722/j.cnki.jrme.2015.1369

Wu A.X., Wang Y., Zhang M.Z., et al. (2021) New Development and Prospect of Key Technology in Underground Mining of Metal Mines. Metal Mine, pp. 1-13. https://doi.org/10.19614/j.cnki.jsks.202101001

Liu H.L., Yang T.H., Zhao Y., et al. (2021) A path for evaluating the mechanical response of rock masses based on deep mining-induced microseismic data: A case study. Tunnelling and Underground Space Technology incorporating Trenchless Technology Research, Vol. 115. https://doi.org/10.1016/j.tust.2021.104025

Naguleswaran N., Sivakugan N., Veenstra R. (2015) Underground Mine Backfilling in Australia Using Paste Fills and Hydraulic Fills. International Journal of Geosynthetics and Ground Engineering, Vol. 1, pp. 1-7. https://doi.org/10.1007/s40891-015-0020-8

Cao S., Song W.D., Xue G.L. (2019) Experimental research on mechanical properties of combined cemented tailings backfill and its application. Journal of Mining & Safety Engineering, Vol. 36, pp. 601-608. https://doi.org/10.13545/j.cnki.jmse.2019.03.022

Chen S.M., Wang Y.M., Wu A.X., et al. (2020) Coupled effects of curing stress and curing temperature on mechanical and physical properties of cemented paste backfill. Construction and Building Materials, Vol. 273. https://doi.org/10.1016/j.conbuildmat.2020.121746

Liu B, Li Q.L., Xu W.B. (2020) Coupled effect of curing temperature and age on compressive behavior, microstructure and ultrasonic properties of cemented tailings backfill. Construction and Building Materials, Vol. 237. https://doi.org/10.1016/j.conbuildmat.2019.117738

Cao C, Cao Y.S., Wang Y., et al. (2023) Effect of Curing Temperature under Deep Mining Conditions on the Mechanical Properties of Cemented Paste Backfill. Minerals, Vol. 13. https://doi.org/10.3390/min13030383

Cai S.J., Wu D. (2015) Coupled effect of cement hydration and temperature on hydraulic behavior of cemented tailings backfill. Journal of Central South University, Vol. 22, pp. 1956-1964. https://doi.org/10.1007/s11771-015-2715-3

Bai Y., Dai Y.Z., Li P., et al. (2020) Study on the Time-varying Law of Temperature Field and Strength of Cemented Paste Backfill at Low Temperature. Journal of Hebei University of Engineering (Natural Science Edition), Vol. 37, pp. 80-87. https://doi.org/10.3969/j.issn.1673-9469.2020.02.013

Ma J., Peng K., Yang Q., et al. (2013) Mix ratio optimization of alpine mine backfill based on the response surface method. Journal of University of Science and Technology Beijing, Vol. 35, pp. 559-565. https://doi.org/10.13374/j.issn1001-053x.2013.05.003

Bian J.W., Chen Y., Hu Y.B., et al. (2015) Orthogonal Test of Optimization of Ultrafine Whole-tailings Backfill Materials. Gold Science and Technology, Vol. 23, pp. 45-49. http://www.goldsci.ac.cn/CN/10.11872/j.issn.1005-2518.2015.03.045

Xiong R. (2015) Effect of High temperature on Strength and Deformation characteristics of cemented backfill. Mining Technology, Vol. 15, pp. 18-21. https://doi.org/10.13828/j.cnki.ckjs.2015.06.008

Han B., Liu C., Sun W., et al. (2015) Optimized mix ratio of crushed waste rocks in cementing backfill and its application in extreme cold weather. Journal of Central South University (Science and Technology), Vol. 46, pp. 4195-4203. https://doi.org/10.11817/j.issn.1672-7207.2015.11.029

Han B., Liu C., Sun W., et al. (2015) Experimental study of Strength of Backfillings of Cemented rock debris and Its application under Low temperature condition. Chinese Journal of Rock Mechanics and Engineering, Vol. 34, pp. 139-147. https://doi.org/10.13722/j.cnki.jrme.2015.01.015

Hao Y.M., Jiao G.R., Yang Z.L., et al. (2020) Influence of Temperature on the Cemented Backfill. Mining Research and Development, Vol. 40, pp. 46-49. https://doi.org/10.13827/j.cnki.kyyk.2020.03.011

Wang W. Zhou P.F. (2022) Experimental Study on Compressive Strength and Failure Mode of Cemented Tailings Backfill at Different Curing Temperatures. Nonferrous Metals Engineering, Vol. 12, pp. 167-176. https://doi.org/10.3969/j.issn.2095-1744.2022.08.022

Fang K., Fall M. (2018) Effects of curing temperature on shear behaviour of cemented paste backfill-rock interface. International Journal of Rock Mechanics and Mining Sciences, Vol. 112, pp. 184-192. https://doi.org/10.1016/j.ijrmms.2018.10.024

Hou C., Yan B.X., Zhu W.C., et al. (2020) The effects of temperature and binder content on the behavior of frozen cemented tailings backfill at early ages. Construction and Building Materials, Vol. 239. https://doi.org/10.1016/j.conbuildmat.2019.117752

Pan Z., Wang Y.M., Zhou K.P., et al. (2022) Comparative Analysis of Strength and Deformation Behavior of Cemented Tailings Backfill under Curing Temperature Effect. Materials, Vol. 15. https://doi.org/10.3390/ma15103491

Jiang R. (2020) Influence of Early Curing Methods on Properties of Ultrahigh-performance Concrete. Journal of the Chinese Ceramic Society, Vol. 48, pp. 1659-1668. https://doi.org/10.14062/j.issn.0454-5648.20200251

Tan Y.Y., Yu X., Zhang K., et al. (2020) The Mechanical and Microstructural Properties of Composite Structures Made of a Cement-Tailing Backfill and Rock Core, Minerals, Vol. 10. https://doi.org/10.3390/min10020159

Wang C.H., Wang J.J., X J.H., et al. (2020) Study on the optimum initial curing condition for fly ash and GGBS based geopolymer recycled aggregate concrete. Construction and Building Materials, Vol. 247. https://doi.org/10.1016/j.conbuildmat.2020.118540

Jiang Z.W., Meng X., Tan Y.Y., et al. (2022) Research on Flocculant Selection for Classified Fine Tailings Based on Micro-Characterization of Floc Structure Characteristics. Materials, Vol. 15. https://doi.org/10.3390/ma15072460

Kong L.W., Zhang X.W. (2013) Study of pore characteristics of offshore clay by SEM and MIP and NA methods. Rock and Soil Mechanics, Vol. 34, pp. 134-142. https://doi.org/10.16285/j.rsm.2013.s2.025

Long G.C., Ma K.L., Xie Y.J., et al. (2021) Hydration and multiscale pore structure characterization of steam-cured cement paste investigated by X-ray CT. Construction and Building Materials, Vol. 282. https://doi.org/10.1016/j.conbuildmat.2021.122629

Li G.C., Liu G.L., Liu S.L. (2021) Effect of Curing Conditions on the Early Mechanical Properties and Microstructure of Cemented Backfill. Nonferrous Metals Engineering, Vol. 11, pp. 83-92. https://doi.org/10.3969/j.issn.2095-1744.2021.08.012

Li Q.L., Xu W.B., Zhang Y.L. (2019) Influence of temperature on compressive strength, microstructure properties and failure pattern of fiber-reinforced cemented tailings backfill. Construction and Building Materials, Vol. 222, pp. 776-785. https://doi.org/10.1016/j.conbuildmat.2019.06.203

Fu J.X., Wang J., Wang K. (2023) Internal pore evolution and early hydration characterization of fly ash cement backfill. Journal of Building Engineering, Vol. 72. https://doi.org/10.1016/j.jobe.2023.106716

Song W.D., Wang J., Zhang C., et al. (2022) Effect of waste glass powder on pore structure, mechanical properties and microstructure of cemented tailings backfill. Construction and Building Materials, Vol. 365. https://doi.org/10.1016/j.conbuildmat.2022.130062

Deng Y.C., Kou Y.P., Tan Y.Y., et al. (2023) Hydration Characteristics and Early Strength Evolution of Classified Fine Tailings Cemented Backfill. Materials, Vol. 16. https://doi.org/10.3390/ma16030963

Acronyms

NMR Nuclear Magnetic Resonance
SEM Scanning Electron Microscope
AFt ettringite
C-S-H Calcium Silicate Hydrate
XRD X-ray diffraction
C_3S tricalcium silicate
C_2S dicalcium silicate
C_3A tricalcium aluminate

UCS uniaxial compressive strength
T2 transverse relaxation time